

Discovery of Light-induced Metastable Martensitic Anomaly Controlled by Single-Cycle Terahertz Pulses

X. Yang^{1†}, B. Song^{1†}, C. Vaswani¹, L. Luo¹, C. Sundahl², M. Mootz³,
J-H. Kang², Y. Yao¹, K-M Ho¹, I. E. Perakis³, C. B. Eom² and J. Wang^{1*}

¹*Department of Physics and Astronomy and Ames Laboratory-U.S. DOE,
Iowa State University, Ames, Iowa 50011, USA.*

²*Department of Materials Science and Engineering,*

University of Wisconsin-Madison, Madison, WI 53706, USA.

³*Department of Physics, University of Alabama at Birmingham, Birmingham, AL 35294-1170, USA.*

(Dated: August 21, 2020)

We report on an ultrafast photoinduced phase transition with a strikingly long-lived Martensitic anomaly driven by above-threshold single-cycle terahertz (THz) pulses in Nb₃Sn. A non-thermal, THz-induced depletion of low frequency conductivity indicates increased gap splitting of high energy Γ_{12} bands by removal of their degeneracies which enhances the Martensitic phase. In contrast, optical pumping leads to a Γ_{12} gap melting. Such light-induced non-equilibrium Martensitic instability persists up to a critical temperature ~ 100 K, i.e., more than twice the equilibrium temperature, and can be stabilized beyond technologically-relevant, nanosecond timescales. Together with first-principle simulations, we identify a compelling THz tuning of structural fluctuations via E_u phonons to achieve a non-equilibrium ordering at high temperatures far exceeding those for equilibrium states.

An emerging paradigm for condensed matter physics is actively explored in light-induced correlation phenomena and phase transitions such as superconductivity [1, 2] and density wave collective orders [3]. It remains a challenge to develop efficient, non-thermal tuning knobs at THz clock rates and stabilize transient photoinduced phases at many nanosecond timescales. In contrast to high energy optical excitation, the advent of intense single- and few-cycle THz pulses with peak fields of more than 1000 kV/cm (red line, Fig. 1a) represents a unique opportunity for phase switching and stabilization by applying a lightwave dynamic symmetry breaking principle [4] with minimal heating of electronic states [5, 6]. A compelling example is the possibility to achieve light-induced superconductivity via multi-THz nonlinear structural pumping in cuprates, which persists far above the equilibrium critical temperatures although it lasts only for few picoseconds [2]. Unlike in these intensely-debated, complex materials, A₃B compounds, such as Nb₃Sn with A15 crystal structure, represent simpler and well-understood model correlated materials [5, 7], which are well suited for seeking examples of non-equilibrium phase transition by using phonon pumping. Such THz lattice driving is still scarce, despite of recent progress [2, 8–13]. Here we use Nb₃Sn to address two outstanding general issues: (i) can intense THz light pump fields create *long-lived* Martensitic orders *far above* equilibrium critical temperatures? (ii) what are the salient features of the non-thermal tuning of structural fluctuations that give rise to such controllable non-equilibrium order?

A Martensitic normal state transition in Nb₃Sn can be understood in terms of electronic and structural instabilities, which associate with optical phonon condensation. As illustrated in Fig. 1a, “dimerization” of Nb atoms emerges along three one-dimensional chains (blue dash

lines) at $T_M=48$ K above the superconducting transition at T_c [14–17]. Such structural (cubic-tetragonal) and phonon softening anomalies can originate from a Van Hove singularity (VHS)-like, electronic density-of-states (DOS) peaked at $\sim E_F$ and from strong electron-phonon interaction. These give rise to a Jahn-Teller effect due to two fold-degenerate Γ_{12} sub-bands crossing the Fermi level, with DOS that determines T_M of the Martensitic phase transition. Therefore, the Γ_{12} phonon pumping by an intense, few-cycle THz-pulse ~ 1000 kV/cm (red trace, Fig. 1a), without significantly heating of other degrees of freedom, provides a compelling avenue to induce a non-equilibrium Martensitic phase at temperatures far exceeding the equilibrium T_M , by lifting the electronic degeneracy and increasing DOS of the Γ_{12} bands. Although quantum quench of superconducting states has been actively explored in Nb₃Sn [5], the THz-driven Martensitic normal states have never been explored which is the focus of this work.

In this letter, we present a light-induced metastable, Martensitic phase out-of-equilibrium in Nb₃Sn obtained by single-cycle THz pumping. The photoinduced non-equilibrium Martensitic phase displays the non-thermal electrostatics that persist up to a critical $T_M^* \sim 2T_M$, i.e., doubling of the equilibrium value, for longer than 1 ns. Our theoretical modeling underpins a Γ_{12} phonon-tuning mechanism of the Martensitic instability and explains, particularly, the doubling of T_M and non-thermal conductivity depletion.

The sample measured in the experiment is a 20nm Nb₃Sn film grown on (100) oriented sapphire single crystalline substrates by pulsed laser deposition. Single cycle THz pump pulses were generated by a tilted-pulse-front phase matching through 1.3% MgO doped LiNbO₃ crystal. Peak E field is as large as 1000 kV/cm (Fig. 1a)

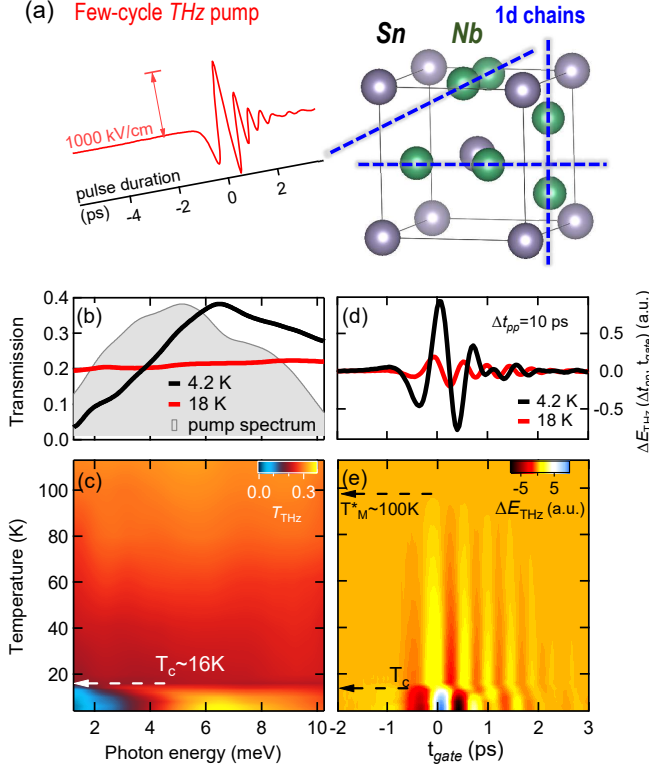


Figure 1. (a) Experimental schematics of driven Martensitic phase with intense THz pulses (red line). (b) Probe transmission $T_{\text{THz}}(\omega)$ through sample shown together with the pump spectra (gray shade). (c) 2D plot of $t_{\omega, T}$ from 4 K to 110 K. (d), (e) THz Pump-induced transmitted field change ΔE_{THz} at temperatures same as (b), (c). Dash line marks the SC transition at $T_c = 16$ K and THz light-induced critical temperature $T_M^* = 100$ K.

and spectrum (gray shade, Fig. 1b) covers ~ 1 -10 meV. Complex transmission $\tilde{t}(\omega)$ is obtained by Fourier spectra of transmitted THz probe field oscillation in time domain. Frequency dependent optical conductivity $\sigma_1(\omega)$ and $\sigma_2(\omega)$ extracted from $\tilde{t}(\omega)$ measures dissipative and inductive response respectively [18–22].

Fig.1b presents the static THz transmission of Nb_3Sn $T(\omega) = |\tilde{t}(\omega)|$ at 4.2K and 18K. quasi-particle (QP) excitation gap $2\Delta_{\text{SC}}$ gives rise to the SC state line shape (black line), while the normal state spectrum (red line) is largely featureless, tilting slightly up towards high frequency. A 2D false-color plot of THz transmission spectra $T(\omega)$ at various temperatures (Fig.1c) shows distinctly different shapes below and above critical temperature $T_c \sim 16$ K. There the transmission peak diminishes and redshifts with increasing temperature, and completely vanishes when approaching T_c . Our focus next is THz pumping of Martensitic normal states above T_c . Fig. 1c shows that equilibrium transmission spectra above T_c show very little changes in the measured

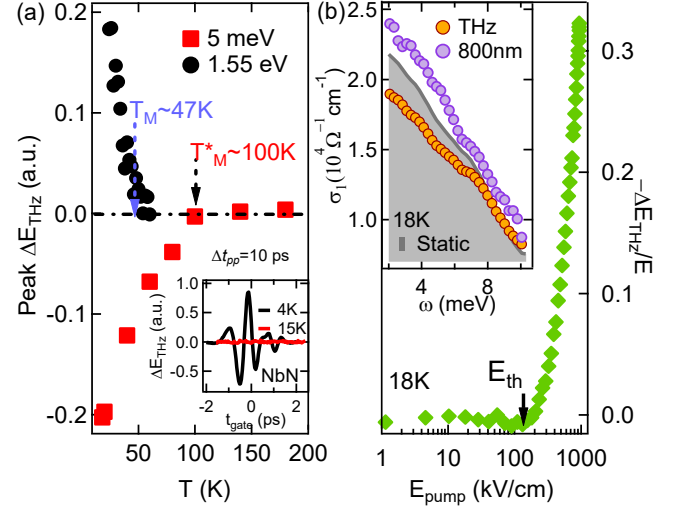


Figure 2. (Color online). (a) Temperature dependence of pump induced change ΔE_{THz} under THz and 1.55eV optical photo-excitation. Martensitic transition temperature T_M and T_M^* for vanishing ΔE_{THz} under THz pump is marked by purple and black arrows, respectively. Inset: No pump induced change is observed in a NbN superconductor above $T_c = 14$ K. (b) Pump field dependence of ΔE_{THz} at 18K shows a threshold E_{th} at 130kV/cm. Inset: Non-equilibrium conductivity $\sigma_1(\omega)$ under THz and 1.55 eV pump compared to thermal equilibrium state at 18K.

frequency range, i.e., the static THz conductivity is not very sensitive to the Martensitic normal state order.

In strong contrast, non-equilibrium signals after THz pump centered at ~ 5 meV show a clear temperature-dependence in the normal state. Fig.1d shows typical pump-induced changes of transmitted field ΔE_{THz} in time domain at $\Delta t_{\text{pp}} = 10$ ps. The normal state, 18K trace shows a clearly phase shift and amplitude reduction in comparison with the 4.2K trace. Fig.1e presents a 2D false plot of ΔE_{THz} up to ~ 110 K. Again, normal state is well separated from SC state across T_c . Most intriguingly, clear ΔE_{THz} signals are detected in the normal state and persist up to 100 K, i.e., $T_M^* \sim 2T_M$, indicative of a photo-induced non-equilibrium order far above T_M .

To further underpin the THz pump-induced T_M^* phase, Fig.2a shows pump-induced differential transmission ΔE_{THz} under conventional optical pump, 1.55eV. Here the optically-induced THz signals (black circles) vanish at the equilibrium transition at $T_M = 48$ K. These results clearly establish ultrafast optically-induced ΔE_{THz} as an effective probe for the equilibrium Martensitic order. In contrast, the 5meV photo-excitation clearly establishes the non-zero ΔE_{THz} signals up to T_M^* , indicative of “order-parameter-like” response for the non-equilibrium Martensitic phase.

Further experimental evidence associating the THz-driven phase transition is presented in Fig. 2b, which

plots THz pump field dependence of ΔE_{THz} signals at a fixed time $\Delta t_{pp} = 10\text{ps}$. It is clearly visible that the signal is negligibly small at THz field strengths less than $E_{\text{th}} \sim 130\text{kV/cm}$ but increases significantly above it. Such distinct threshold behavior of the THz-driven dynamics is not limited by our noise floor, which is a hallmark of the non-equilibrium phase transition to an induced Martensitic phase. For comparison, no THz pump-induced change is observed in a NbN superconductor in the normal state without the Martensitic order, e.g., the 15K trace in (red line, inset, Fig. 2a) for NbN vs the 18K trace (red line, Fig. 1d) for Nb₃Sn.

The non-equilibrium response function $\sigma_1(\omega)$ in Fig. 2(b) (inset) reveals different behaviors for 1.55eV (optical, purple) and 5meV (THz, orange) pumping, which distinguish thermal vs non-thermal electro-dynamics. After high photon energy, 1.55eV pump excitation, the low frequency conductivity gains an additional spectral weight over its equilibrium (no pump) values (gray shade), i.e., $\Delta\sigma_1(\omega) > 0$. This can be understood as melting of the high energy electronic gaps that develop at the T_M transition from Γ_{12} phonon condensation (dimerization). The latter leads to spectral weight transfer to the Fermi surface by suppressing the Martensitic phase via hot phonons and electrons excited by the high energy photons. However, the 5meV pump photon energy is far below the gap and thus cannot quench it. Instead, it reverses the spectral weight transfer to high energy by reducing $\sigma_1(\omega)$. This is consistent with an elevated transition temperature T_M^* and, thereby, enhanced non-equilibrium Martensitic order by acquiring an extra spectral weight from the Fermi surface, as quantitatively substantiated latter.

Fig. 3 presents extensive conductivity spectra measurement and spectral weight (SW) analysis in the normal state to investigate Martensitic dynamics under intense THz radiation. The integrated SW change ΔSW (1-10 meV) induced by the THz pumping is shown in Fig. 3a at various temperatures in the normal state, together with complex conductivity spectra, $\sigma_1(\omega)$ and $\sigma_2(\omega)$, shown in Figs. 3b-3e. The most salient feature is the depleted SW, i.e., $\Delta\text{SW} < 0$, that emerges elusively below T_M^* . Such SW removal in $\sigma_1(\omega)$ corresponds to a reduction in $\sigma_2(\omega)$ (inset) as compared to thermal-equilibrium states (gray crosses, Figs. 3b-3e), which is correlated by Kramers-Kronig transformation. Since the total integrated SW is conserved, the missing spectral component is expected to transfer to high energy electronic states beyond the measurement energy window, which gives rise to a transient increase of T_M to T_M^* . Such experimental evidence indicates strong correlation between THz-controlled SW transfer and Martensitic order. Furthermore, the T_M^* phase appears to be metastable, as witnessed by the long ~ 1 ns relaxation time, e.g., as shown in 620kV/cm trace (black line) in Fig. 3f.

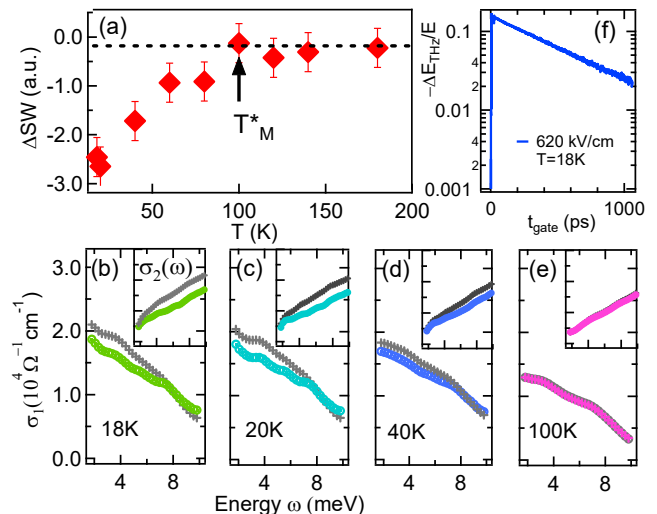


Figure 3. (Color online). (a) Spectral weight change ΔSW integrated from 2-10meV under highest driving field of THz excitation. (b)-(e): Real part of conductivity $\sigma_1(\omega)$ compared to thermal equilibrium at various temperatures with $\sigma_2(\omega)$ shown in inset. (f) $\Delta E_{\text{THz}}/E$ temporal dynamics at $E_{\text{THz}}=620\text{kV/cm}$ and 18K.

The effects of THz field interaction with the Martensitic phase in Nb₃Sn can be understood by considering degenerate Γ_{12} electronic bands crossing the Fermi level (inset, Fig. 4a) and strong electron-phonon coupling [15, 16, 23–25]. Two degenerate E_u phonon modes involved are shown in Fig. 4b (inset). It has been proposed that the transition temperature T_M is proportional to the DOS of Γ_{12} electronic bands at the Fermi level [16]. Our physical picture and simulations below demonstrate that Γ_{12} lattice vibration driven by low energy photo-excitation close to E_u phonon resonances is able to lift the degeneracy and modify the DOS of the Γ_{12} band, as illustrated in Fig. 4a (inset). Active modulations of the Martensitic transition temperature, correlation gap and electronic order are achieved by intense THz radiation, which is absent for high energy, optical pumping with photon energy far above the E_u phonon resonances. The Γ_{12} lattice vibration most relevant to the Martensitic phase can be understood as dimerization of the Nb atom chain along different axes (E_u symmetry, inset, Fig. 4b) similar to a charge density wave but confined to a single unit cell with wave vector $q = 0$.

To put the above-mentioned physical picture on a sound footing, we lay out first-principle simulations of the phonon-assisted tuning of the Martensitic phase (see Supplementary for details). The Γ_{12} phonon contains two degenerate modes at Γ point in B.Z., which are (deduced

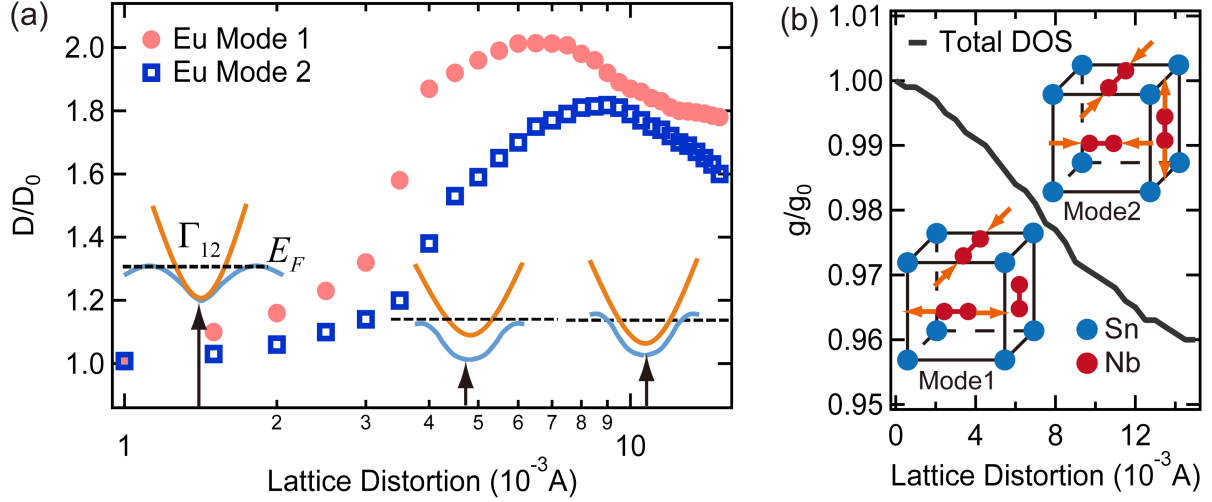


Figure 4. (Color online). (a) DOS (D) of two equivalent Γ_{12} electronic bands and (b) total DOS (g) at Fermi level under finite lattice distortions (compared to its equilibrium D_0 , g_0). Inset in (a): the schematic of Γ_{12} bands under lattice distortion. Inset in (b): Two E_u phonon modes are manifested as lattice vibration of Nb atoms in chains along three different directions.

from symmetry)

$$\begin{aligned} Q_1 &= \frac{A_1}{2}(-u_{2x} + u_{1x} + u_{4y} - u_{3y}) \\ Q_2 &= \frac{A_2}{2\sqrt{3}}(2u_{6z} - 2u_{5z} - u_{2x} + u_{1x} - u_{4y} + u_{3y}) \end{aligned} \quad (1)$$

$u_{i\sigma}$ stand for the displacement of i^{th} Nb atoms in the σ Cartesian component. The x -coordinates in Fig. 4 correspond to A_1 and A_2 in the above equations.

The total free energy can be constructed based on the two E_u modes

$$\begin{aligned} F &= \frac{1}{2}Vc_0u^2 + \frac{1}{2}\omega^2(Q_1^2 + Q_2^2) + \zeta\sqrt{Vc_0}\omega uQ_1 \\ &\quad + Vn\mu - 2k_B T(S_{b1} + S_{b2}), \end{aligned} \quad (2)$$

where V is unit cell volume, c_0 is force constant, μ is chemical potential, and u is defined by

$$u = (2e_{zz} - e_{xx} - e_{yy})/\sqrt{6}, \quad (3)$$

where e_{xx} , e_{yy} , e_{zz} are the diagonal components of strain tensors. S_{b1} and S_{b2} are the entropy due to the two Γ_{12} electronic bands, which are expressed as

$$S_{iB} = \sum_k \ln[1 + \exp[-(\varepsilon_k^i - \mu)/k_B T]] \quad (4)$$

The zero order H_0 of band energies ε_k can be simplified as parabolic, which are plausible approximations for dispersion near the Γ point in B.Z. It will be perturbed by the following Hamiltonian $H_e = H_0 + H'$

$$\begin{aligned} H' &= \left[\frac{\eta_i \omega}{\sqrt{nV}} Q_2 + \frac{\hbar^2}{2m} \frac{1}{\sqrt{2}} (k_x^2 - k_y^2) \right] (c_1^\dagger c_2 + c_2^\dagger c_1) \\ &\quad + \left[\eta_0 \sqrt{\frac{c_0}{n}} u + \frac{\eta_i \omega}{\sqrt{nV}} Q_1 + \frac{\hbar^2}{2m} \frac{1}{\sqrt{6}} (3k_z^2 - k^2) \right] (c_2^\dagger c_2 - c_1^\dagger c_1) \end{aligned} \quad (5)$$

In above, we have ignored the k index for c_1 c_2 , etc. Note that η_0 , η_i come into F through ε_k^i .

In order to account for the Martensitic transition, the model has included several degrees of freedom: the elastic distortion (tensor) u , optical phonon modes Q_1 Q_2 , electron entropy, and e -phonon coupling. Minimize F with respect to u , Q_1 , Q_2 and μ , yielding the equilibrium lattice displacement, which relies on numerical solutions. It shows that the critical T_M is approximately proportional with a parameter α in a broad regime, i.e., $k_B T_M / \varepsilon_F \propto \alpha$.

$$\begin{aligned} \alpha &= 2a_0^3 D(\varepsilon_F) G_0^2, \\ G_0 &= |\eta_0| \sqrt{1 + \frac{(\eta_i - \zeta \eta_0)^2}{(1 - \zeta^2) \eta_0^2}} \end{aligned} \quad (6)$$

$D(\varepsilon_F)$ is Γ_{12} density of states at Fermi level, and a_0 is the lattice parameter of undistorted unit cell (cubic). Notice that a_0 and G_0 could largely be taken as constant, then it yields, $T_M \propto \alpha \propto D(\varepsilon_F)$.

Next, we explicitly evaluate Γ_{12} -DOS change with presence of Γ_{12} phonon modes. The electronic structure under Γ_{12} lattice distortion is examined by density functional theory (DFT) [26] with PAW methods [27] and Perdew-Burke-Ernzerhof (PBE) exchange-correlation functional [28] using the ‘‘Frozen phonon’’ approximation. Our results are presented in Fig.4a, which

shows the DOS of Γ_{12} electronic bands at the Fermi level (FL) vs phonon amplitudes of the characterized by Nb atom displacement from its equilibrium position. Note that Fig.4a only accounts for the DOS due to the Γ_{12} bands, which is different from total DOS (Fig. 4b). Strikingly, DOS of Γ_{12} bands undergoes a sharp increase above threshold at 0.002\AA and reaches a maximum two-time enhancement at displacement as small as 0.006\AA , followed by a slight drop under further distortion. The sudden increase is due the band (blue in Fig. 4a) that touches and crosses the FL at a critical amplitude, leading to an approximate doubling of the Γ_{12} -DOS. Thus, simulations well address the experimental observation of two-time enhancement in transition temperature $T^* \simeq 2T_M$ and also implies a threshold E field (~ 130 kV/cm) for enhanced T_M , as observed in Fig. 2a. On the other hand, in Fig. 4b, the decrease in the total DOS, i.e., $\sim 4\%$ in the whole range of phonon distortions, is in excellent agreement with the decreased SW in THz driven states below T_M^* observed in Figs. 3b-3e. Furthermore, our DFT calculation shows E_u phonon energy ~ 12 meV, which is an overestimate since it cannot fully capture electron-phonon interaction near the Martensitic transition [29]. Nevertheless, the E_u phonon energy is clearly close the THz pump pulse up to ~ 10 meV, which can excite the Γ_{12} resonance non-thermally.

In summary, we demonstrate a light-enhanced Martensitic phase driven by intense, single-cycle THz fields, manifested as the doubling of transition temperature and removal of spectral weights in the vicinity of the Fermi level. First-principle calculations reveal an effective non-thermal modulation of degenerate Γ_{12} electronic bands that determine the Martensitic phase and consistently explain all the key experimental features. The light-induced phonon tuning can be extended to topological matter [30], 2D materials [31], magnetism [32, 33] and unconventional superconductors [34, 35]. Our work also provides compelling implications for quantum computation applications since doped Nb_3Sn is still the material of choice to replace Al-based transmon qubits and support high current/magnetic field applications, despite of much improved T_c in unconventional superconductors.

This work was supported by National Science Foundation 1905981 (THz spectroscopy). B.S. and L.L. (DFT calculation and model building) were supported by the U.S. Department of Energy, Office of Basic Energy Science, Division of Materials Sciences and Engineering (Contract No. DE-AC02-07CH11358). Work at the University of Wisconsin was supported by the Department of Energy Office of Basic Energy Sciences under award number DE-FG02-06ER46327 (structural and electrical characterizations) and Department of Energy Grant no. DE-

SC100387-020 (sample growth). Data analysis work at the University of Alabama, Birmingham was supported by the US Department of Energy under contract # DE-SC0019137 (M.M and I.E.P). The THz Instrument was supported in part by National Science Foundation EECS 1611454.

*Corresponding author: jwang@ameslab.gov.

† Equal contribution

-
- [1] Yang, X. et al. *Nat. Photon.* **13**, 707 (2019)
 - [2] Fausti, D. et al. *Science* **331**, 189-192 (2011).
 - [3] Patz, A. et al. *Nat. Commun.* **5**, 3229 (2014).
 - [4] C. Vaswani et al., *Phys. Rev. Lett.* **124**, 207003 (2020).
 - [5] Yang, X. et al. *Nat. Mater.* **17**, 586-591 (2018)
 - [6] Dienst, A. et al. *Nat. Photonics.* **5**, 485-488 (2011).
 - [7] Yang, X. et al. *Phys. Rev. B* **99**, 094504 (2018)
 - [8] M. Kozina, M. Fechner, P. Marsik, T. van Driel, J. M. Glowina, C. Bernhard, M. Radovic, D. Zhu, S. Bonetti, U. Staub, M. C. Hoffmann, *Nat. Phys.*, **15**, 387 (2019)
 - [9] X. Li, T. Qiu, J. Zhang, E. Baldini, J. Lu, A. M. Rappe, and K. A. Nelson, *Science*, **364**, 1079 (2019)
 - [10] E. Sie et al., *Nature* **565**, 61 (2019).
 - [11] Vaswani, C. et al., *Phys. Rev. X* **10**, 021013 (2020)
 - [12] Liu, Z. et al., *Phys. Rev. Lett.* **124**, 157401 (2020)
 - [13] X. Yang et al., *npj Quantum Mater.*, **5**, 13 (2020). <https://doi.org/10.1038/s41535-020-0215-7>
 - [14] Shirane, G. and Axe, J. D. *Phys. Rev. B* **4**, 2957 (1971).
 - [15] G. Bilbro, and W. L. McMillan, *Phys. Rev. B*, **14**, 1887 (1976)
 - [16] M. Kataoka, *Phys. Rev. B*, **28**, 2800 (1983)
 - [17] B. Sadigh, and V. Ozolis. *Phys. Rev. B*, **57**, 2793 (1998)
 - [18] Luo, L. et al. *Nat. Commun.* **5**, 3055 (2014).
 - [19] Luo, L. et al. *Nat. Commun.* **8**, 15565 (2017).
 - [20] Wang, J. et al. *Phys. Rev. Lett.*, **104**, 177401 (2010).
 - [21] Luo, L. et al. *Phys. Rev. Lett.*, **114**, 107402 (2015).
 - [22] Luo, L. et al. *Phys. Rev. Materials*, **3**, 026003 (2019).
 - [23] L. P. Gor'kov, *Inst. of Theoretical Physics, Moscow*, **65**, 1658 (1973)
 - [24] R. N. Bhatt, and W. L. McMillan. *Phys. Rev. B*, **14**, 1007 (1976)
 - [25] R. N. Bhatt, *Phys. Rev. B*, **16**, 1915 (1977)
 - [26] A. T. Van Kessel, H. W. Myron, and F. M. Mueller. *Phys. Rev. Lett.* **41**, 3. 181 (1978).
 - [27] P. E. Blochl, *Phys. Rev. B* **50**, 17953 (1994)
 - [28] L.F. Mattheiss, and W. Weber. *Phys. Rev. B*, **25**, 2248 (1982)
 - [29] H. M. Tutuncu, G. P. Srivastava, S. Bagci, and S. Duman. *Phys. Rev. B* **74**, 212506 (2006).
 - [30] L. Luo et al., *Nat. Commun.* **10**, 607 (2019).
 - [31] See, e.g., T. Li, et al. *Phys. Rev. Lett.* **108**, 167401 (2012).
 - [32] T. Li et al., *Nature* **496**, 69 (2013)
 - [33] A. Patz, T. Li, X. Liu, J. K. Furdyna, I. E. Perakis, and J. Wang, *Phys. Rev. B* **91**, 155108 (2015).
 - [34] X. Yang et al., *Phys. Rev. Lett.* **121**, 267001 (2018)
 - [35] Patz, A. et al. *Phys. Rev. B* **95**, 165122 (2017)